

## Location and dimensionality estimation of geological bodies using eigenvectors of "Computed Gravity Gradient Tensor"

Karimi, K.<sup>1\*</sup>, Oveysi Moakhar, M.<sup>2</sup> and Shirzaditabar, F.<sup>2</sup>

1. M.Sc. Student, Department of Physics, faculty of Science, Razi University, Kermanshah, Iran

2. Assistant Professor, Department of Physics, faculty of Science, Razi University, Kermanshah, Iran

(Received: 11 March 2018, Accepted: 15 May 2018)

### Abstract

One of the methodologies employed in gravimetry exploration is eigenvector analysis of Gravity Gradient Tensor (GGT) which yields a solution including an estimation of a causative body's Center of Mass (COM), dimensionality and strike direction. The eigenvectors of GGT give very rewarding clues about COM and strike direction. Additionally, the relationships between its components provide a quantity ( $I$ ), representative of a geologic body dimensions. Although this procedure directly measures derivative components of gravity vector, it is costly and demands modern gradiometers. This study intends to obtain GGT from an ordinary gravity field measurement ( $g_z$ ). This Tensor is called Computed GGT (CGGT). In this procedure, some information about a geologic mass COM, strike and rough geometry, just after an ordinary gravimetry survey, is gained. Because of derivative calculations, the impacts of noise existing in the main measured gravity field ( $g_z$ ) could be destructive in CGGT solutions. Accordingly, to adjust them, a "moving twenty-five point averaging" method, and "upward continuation" are applied. The methodology is tested on various complex isolated and binary models in noisy conditions. It is also tested on real geologic example from a salt dome, USA, and all the results are highly acceptable.

**Keywords:** Computed Gravity Gradient Tensor (CGGT); Dimensionality Index ( $I$ ); Eigenvector; Eigenvalue.

### 1. Introduction

Nabighian (1984) extended the 2D Hilbert Transform of a potential field to 3D cases, in which he proved that Hilbert Transform was composed of two parts: one acting on x component, and another, on y component. Having this knowledge, each horizontal and vertical components of the potential field are derivable from each other. On the other hand, gravity gradiometry goes historically back to 1886, and was a turning point in petroleum industry (Bell and Hansen, 1998). In 1970s, new gradiometers were developed to measure all components of the Gravity Gradient Tensor (GGT) (Bell et al., 1997). Different applications of GGT data have been reported in recent years (Vasco and Taylor, 1991; Pawlowski, 1998; Hatch, 2004; Fedi et al., 2005; Dransfield, 2007). In the last three decades, other processing and interpretation techniques of GGT data have been widely improved (Pedersen and Rasmussen, 1990; Edwards et al., 1997; Childers et al., 1999; Routh et al., 2001; Hinojosa and Mickus, 2002; Zhdanov et al., 2004; While et al., 2006; Droujinine et al., 2007; Murphy and

Brewster, 2007; Pajot et al., 2008; FitzGerald et al., 2009; While et al., 2009; Beiki and Pedersen, 2010; Oruc, 2010; Zhou, 2016). Pedersen and Rasmussen (1990) studied gradient tensors of gravity and magnetic fields and presented some invariants to show source dimensionalities. They also indicated that the maximum eigenvalue and its corresponding eigenvector (first eigenvector) of the GGT are related to the COM of a simple point source. However, they did not develop a practical technique for estimating source location from the first eigenvectors. Furthermore, they neglected the interpretive power contained in the eigenvector corresponding to the minimum eigenvalue (third eigenvector). Zhang et al. (2000) showed that the components of the gradient tensor can be used to improve the Euler deconvolution method. They applied their method on the measured GGT data and improved the performance of Euler deconvolution using all measured gradients. Seven years later, Mikhailov et al. (2007) combined scalar invariants of the tensor and

\*Corresponding author:

kuroshkarimi88@gmail.com

Euler deconvolution to locate equivalent sources. They also proved that tensor deconvolution approximately locates COM, whereas Euler deconvolution better outlines the edges of causative bodies. Oruc (2010) proposed a new method based on the invariants of the GGT to interpret gravity data due to simple causative sources. He estimated the depth of a body from the multiplication of the maximum of the vertical gravity component by the maximum value of a ratio of the invariants related to dimensionality of the body. Beiki and Pedersen (2010) located the causative bodies from a collection of eigenvectors of the GGT using robust least squares. They used the third eigenvectors which provide information about the strike direction of 2D causative bodies. Finally, Zhou (2016) presented a new depth estimation method based on the ratio of gravity and full tensor gradient invariant. In this paper, in place of using directly measured GGT components, they are computed from measured gravity data (CGGT). Then, COMs, strikes, and dimensions of different models are estimated.

## 2. Theory

Due to the fact that the gravity gradiometry and full use of GGT characteristics may be expensive and inconvenient in some geophysical explorations, they are going to be calculated from the vertical component of gravity field ( $g_z$ ) that could be easily measured in an ordinary gradiometry survey. To this end, Hilbert Transform is used, and the other components of gravity vector ( $g_x$  and  $g_y$ ) are acquired. Then, the first derivatives of these three components are calculated (employing Fourier Domain). The horizontal and vertical derivatives of potential field,  $U$ , are Hilbert transforming pairs (Nabighian, 1984):

For 2-D cases

$$\begin{cases} \frac{\partial U}{\partial z} = \mathcal{H}\left(\frac{\partial U}{\partial x}\right) \\ \mathcal{F}\left(\frac{\partial U}{\partial z}\right) = -i \frac{k}{|k|} \mathcal{F}\left(\frac{\partial U}{\partial x}\right) \end{cases} \quad (1)$$

and for 3-D case

$$\begin{cases} \frac{\partial U}{\partial z} = \mathcal{H}(\nabla_{\text{horizontal}} U) \\ \mathcal{F}\left(\frac{\partial U}{\partial z}\right) = -i \frac{k_x}{|k|} \mathcal{F}\left(\frac{\partial U}{\partial x}\right) - i \frac{k_y}{|k|} \mathcal{F}\left(\frac{\partial U}{\partial y}\right) \end{cases} \quad (2)$$

where  $\mathcal{H}$  is Hilbert transform operator and

$$\nabla_{\text{horizontal}} = \frac{\partial}{\partial x} \hat{i} + \frac{\partial}{\partial y} \hat{j}$$

Using inversion of Equation (2) we have (Nabighian, 1984):

$$\begin{cases} g_x = \frac{\partial U}{\partial x} = \mathcal{F}^{-1}\left[i \frac{k_x}{k} \frac{\partial U}{\partial z}\right] \\ g_y = \frac{\partial U}{\partial y} = \mathcal{F}^{-1}\left[i \frac{k_y}{k} \frac{\partial U}{\partial z}\right] \end{cases} \quad (3)$$

Now, CGGT components can be derived as:

$$\mathbf{g}_{mn} = \mathcal{F}^{-1}(ik_m[\mathcal{F}(\mathbf{g}_n)]) \quad (4)$$

Where

$$\begin{cases} m : x, y, z \\ n : x, y, z \end{cases} \quad \mathbf{\Gamma} = \mathbf{GGT} = \mathbf{CGGT} = \begin{bmatrix} g_{xx} & g_{xy} & g_{xz} \\ g_{yx} & g_{yy} & g_{yz} \\ g_{zx} & g_{zy} & g_{zz} \end{bmatrix} \quad (5)$$

Notice that GGT and CGGT are not exactly the same, specifically, in real cases. However, CGGT could be an acceptable estimation of GGT. The components of GGT (measured components by modern gradiometers) have some advantages over those of CGGT (computed components) like fairly noise resistance. It should be noted again that this paper is going to use CGGT, not GGT.

Since  $\mathbf{\Gamma}$  is a symmetrical matrix, it has real eigenvalues ( $b_i$ ) and perpendicular eigenvectors " $\mathbf{v}_i$ ". Therefore, the following relation holds:  $\mathbf{\Gamma}\mathbf{v}_i = b_i\mathbf{v}_i$ .

$\mathbf{\Gamma}$  can then become diagonal by its eigenvectors (Pedersen and Rasmussen, 1990):

$$\mathbf{v}^{-1}\mathbf{\Gamma}\mathbf{v} = \mathbf{A} = \begin{bmatrix} b_3 & 0 & 0 \\ 0 & b_2 & 0 \\ 0 & 0 & b_1 \end{bmatrix} \quad (6)$$

For 2-D cases:  $|b_1|=|b_3|$  and  $b_2=0$ , and for 3-D cases:  $|b_2|=|b_3|$  and  $b_1=2|b_2|=2|b_3|$ . For simplicity in the calculations, instead of “ $\Gamma$ ”, one can work with “ $A$ ”. In a source free region “ $A$ ” has some special features as follows (Pedersen and Rasmussen, 1990):

$$I_0 = \text{Trace}(\mathbf{A}) = \sum_{i=1}^3 \Gamma_{ii} = b_1 + b_2 + b_3 = 0,$$

$$I_1 = A_{11}A_{22} + A_{11}A_{33} + A_{22}A_{33} = b_3b_2 + b_3b_1 + b_2b_1,$$

$$I_2 = \det(\mathbf{A}) = b_3b_2b_1$$

$$0 \leq I = -\left( \frac{\left( \frac{I_2}{2} \right)^2}{\left( \frac{I_1}{3} \right)^3} \right) \leq 1 \quad (7)$$

$I$  is a dimensionality index:  $I=0$  is defined for absolutely 2-D masses, while in the case of a pure 3-D body, it is 1. Predictably, the values between these two belong to geometrically complex bodies. A threshold value, between two and three dimensionality, is defined as  $I=0.5$  (Beiki and Pedersen, 2010). If  $I$  is larger than 0.5, the mass is regarded as a semi-3D one, and vice versa if it is smaller than 0.5.

The first eigenvectors of  $\Gamma$ , corresponding to the largest eigenvalues, approximately point in the center of mass of a body. To explain the convergence of these first eigenvectors to the COM, one can argue that because  $\Gamma$  is symmetrical, one of its eigenvectors, which we call it “first eigenvector”, at each measurement point, approximately aims to the source of the gravitational field (COM), and the other eigenvectors lie in a plane perpendicular to that first eigenvector. On the

other hand, the magnitude of  $\nabla(g_z) = \begin{bmatrix} g_{xz} \\ g_{yz} \\ g_{zz} \end{bmatrix}$

(the third column of  $\Gamma$ ), is approximately two times larger than  $\nabla(g_x) = \nabla(g_y)$ . After diagonalization through Equation (6),  $\nabla(g_z)$  fits the first eigenvector. It stands to reason that eigenvalue of such a rotated vector is twice that of the others, i.e.  $b_1 = 2|b_2| = 2|b_3|$ . The vector passing through each data point

corresponding to the first eigenvector creates a distance with the real COM, which we are looking for. These distances are (Beiki and Pedersen, 2010):

$$\Delta\delta_i = |\mathbf{v}_{1,i} \times (\mathbf{r}_0 - \mathbf{r}_i)| \quad (8)$$

where

$$\mathbf{v}_{1,i} = \frac{1}{R'} [x_i - x'_{i,0}, y_i - y'_{i,0}, z_i - z'_{i,0}]$$

in which  $R' = \sqrt{(x_i - x'_{i,0})^2 + (y_i - y'_{i,0})^2 + (z_i - z'_{i,0})^2}$ . “ $\mathbf{v}_{1,i}$ ” is the first eigenvector in the  $i^{\text{th}}$  point.  $\mathbf{r}_0$  and  $\mathbf{r}_i$  are the coordinates of real COM of a body and  $i^{\text{th}}$  data point, respectively. The point  $(x'_{i,0}, y'_{i,0}, z'_{i,0})$  is a point along “ $\mathbf{v}_{1,i}$ ” that creates the distance  $\Delta\delta_i$  with  $\mathbf{r}_0$ .  $R'$  is the magnitude of the vector in direction of “ $\mathbf{v}_{1,i}$ ” that approximately points to the COM and gives the distance to it. By minimizing the square distances of  $\Delta\delta_i$ , the COM is estimated as (Aster et al., 2003):

$$\mathbf{m}^{\text{est}} = (\mathbf{G}^T \mathbf{G})^{-1} \mathbf{G}^T \mathbf{d} \quad (9)$$

where:

$$\mathbf{d} = \begin{bmatrix} \mathbf{d}_1 \\ \mathbf{d}_2 \\ \vdots \\ \mathbf{d}_i \\ \vdots \\ \mathbf{d}_N \end{bmatrix}, \mathbf{G} = \begin{bmatrix} \mathbf{G}_1 \\ \mathbf{G}_2 \\ \vdots \\ \mathbf{G}_i \\ \vdots \\ \mathbf{G}_N \end{bmatrix}, \quad (10)$$

$$\mathbf{d}_i = \mathbf{G}_i \mathbf{r}_i = \begin{bmatrix} 0 & -\mathbf{v}_{z,i} & \mathbf{v}_{y,i} \\ \mathbf{v}_{z,i} & 0 & -\mathbf{v}_{x,i} \\ -\mathbf{v}_{y,i} & \mathbf{v}_{z,i} & 0 \end{bmatrix} \begin{bmatrix} x_i \\ y_i \\ z_i \end{bmatrix}$$

$$\text{cov}[\mathbf{m}^{\text{est}}] = \begin{bmatrix} c_{11} & c_{12} & c_{13} \\ c_{21} & c_{22} & c_{23} \\ c_{31} & c_{32} & c_{33} \end{bmatrix} \quad (11)$$

and the Standard Error is

$$s = \sqrt{c_{11} + c_{22} + c_{33}} \rightarrow S_{\text{normalized}} = \frac{s}{z_0} \quad (12)$$

where “ $z_0$ ” is the “depth component” of “ $\mathbf{m}^{\text{est}}$ ” (Beiki and Pedersen, 2010).

### 3. Work Flow

The first step is using Hilbert Transform to compute  $g_x$  and  $g_y$  from  $g_z$ . Calculating its components, CGGT is created afterwards. On the basis of the maximum or minimum point of calculated  $g_{zz}$  component of CGGT, centre of an imaginary window, comprising a number of data points, is specified. The dimensions of window are then changed until a solution with a Minimum Standard Error (MSE) is attained (Beiki and Pedersen, 2010).

### 4. Synthetic models

In order to test the capability of this method, six isolated models: sphere, prism, vertical cylinder, 3D vertical dike, infinite horizontal cylinder and 2D vertical dike are considered. The dimensions of the medium and cell size are  $200 \times 200 \text{ m}^2$  and  $5 \times 5 \text{ m}^2$ ,

respectively. The interference effect is also studied using two binary systems in which irregularly shaped models as well as transversely horizontal cylinders in different depths are used. Herein, a binary system is a collection of two juxtaposed models (Figure 1(b) and 1(c)). Such systems are considered to examine how the gravitational response of the models and the precision of the offered method undergo changes. Furthermore, by considering the interfering masses, this study intends to evaluate whether the solutions resulted from this methodology are still applicable and trustable. In all cases, 15% random Gaussian Noise is imposed on the model's main gravity field. The characteristics of models and obtained solutions are given in Table 1. Figure 1(a) shows all the models.

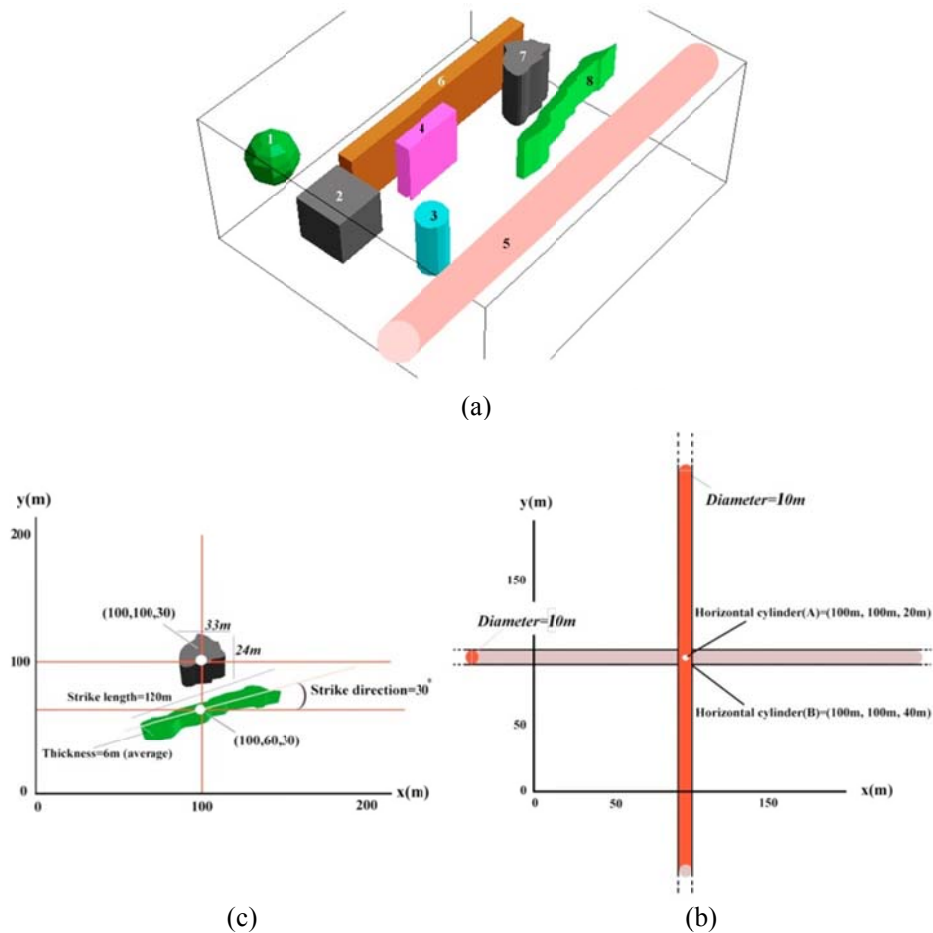


**Figure 1.** a) Schematic images of geophysical models: (1) sphere, (2) prism, (3) vertical cylinder, (4) vertical dike (A), (5) infinite horizontal cylinder used in a solitary and binary analysis, (6) vertical dike (B), (7) and (8) two complex models used in a binary system; b) A binary system of complex models in a virtually horizontal neighborhood; c) A binary system of infinite horizontal cylinders in a vertical adjacency. Real COM (white circles), their relevant coordinates and geometrical properties of the models are shown in (b) and (c).

**4-1. Three dimensional bodies**

Sphere, prism and finite vertical cylinder are examples of 3-D bodies and vertical dike (A) represents a semi 3-D one. To moderate noise effects to a great extent, firstly, a “moving twenty five point averaging” method is employed. In this method, the average of a  $g_z$  data point and its twenty four surrounding points is calculated in a grid map and the average is imputed to the main data point. Secondly, the data are continued upward by 3 meters. Figures 2(a-d) show the  $g_{zz}$  map for sphere, prism, vertical cylinder and vertical dike (A)

in noisy condition (15%). The most suitable window yielding MSE is shown in Figure 2(a). White circles indicate the real COMs and black circles show the estimated ones. In order to examine interference effects, two complex 3D and 2D structures (models (7) and (8) in Figure 1(a)) close together are considered (Table 1 and Figure 1(b)). Because the 3D body’s field is dominant, the maximum point of  $g_{zz}$  contour map roughly lies over it. However, the field effect of neighboring 2D body can disrupt the field and the estimated solutions (see Figure 2(e) and Table 1).

**Table 1.** Geometrical properties of the isolated and binary models in conjunction with the attained solutions.

* N: Number / M:Model / R:Radius / T:Thickness / SL: Strike Length / RSD : Real Strike Direction / DE: Depth Extent / ESD: Estimated Strike Direction											
N	*	M	R (m)	T (m)	SL (m)	RSD [ $\Theta$ (degree) or (x,y,z)]	DE (m)	COM (m)	ESD (x,y,z)	Estimated COM (m)	I
1		Sphere	15	-	-	-	-	(100, 100, 30)	-	(99.8±0.0,99.8±0.0,31.6±0.1)	1.0
2		Prism	-	20, 20	-	-	20	(100,100,30)	-	(99.8±0, 99.8±0, 31.7±0.1)	1.0
3		Vertical cylinder	10	-	-	-	40	(100,100,30)	-	(99.8±0.0, 99.8±0.0, 31.1±0.1)	1.0
4		Vertical dike (A)		10	40	[ $\Theta=0^\circ$ or (1.00, 0.00, 0.00)]	40	(100,100,30)	-	(100±0.1, 99.7±0.2, 25.3±0.1)	0.92
5		Horizontal Cylinder	15	-	2000	[ $\Theta=0^\circ$ or (1.00, 0.00, 0.00)]	-	(100,100,30)	(0.99, 0.00, 0.01)	(99.4±0.6, 99.7±0.6, 31.7±1.8)	0.01
6		Vertical dike (B)	-	10	150	[ $\Theta=60^\circ$ or (0.50,0.86,0.00)]	40	(100,100,30)	(0.50, 0.86, 0.01)	(100.2±0.9, 99.9±1.4, 27.0±1.1)	0.12
2		Prism(A)						(100,100,30)		(99.8±0.1, 99.7±0.1, 32.2±0.1)	1.0
2		Prism(B)	-	30, 30			30	(100,100,40)	-	(99.9±0.1, 99.7±0.1, 37.7±0.1)	1.0
2		Prism(C)						(100,100,50)		(100±0.1, 99.7±0.1, 45.3±0.2)	0.99
8	Binary System	Dike-like	-	6 (ave)	120	[ $\Theta=30^\circ$ or (0.86,0.50,0.00)]	30	(100,60,30)	-	(99.6±0.1, 94.3±0.1, 32.3±0.4)	0.99
7		Cylinder-Like	-	24&33	-	-	40	(100,100,30)			
5	Binary System	Horizontal cylinder (A)	5	-	2000	[ $\Theta=90^\circ$ or (0.00,1.00,0.00)]	-	(100, 100, 20)	(0.00,0.99, .01)	(99.8±1.2, 99.8±1.0, 32.3±1.6)	0.39
5		Horizontal cylinder (B)	5	-	2000	[ $\Theta=0^\circ$ or (1.00,0.00,0.00)]	-	(100, 100, 40)			

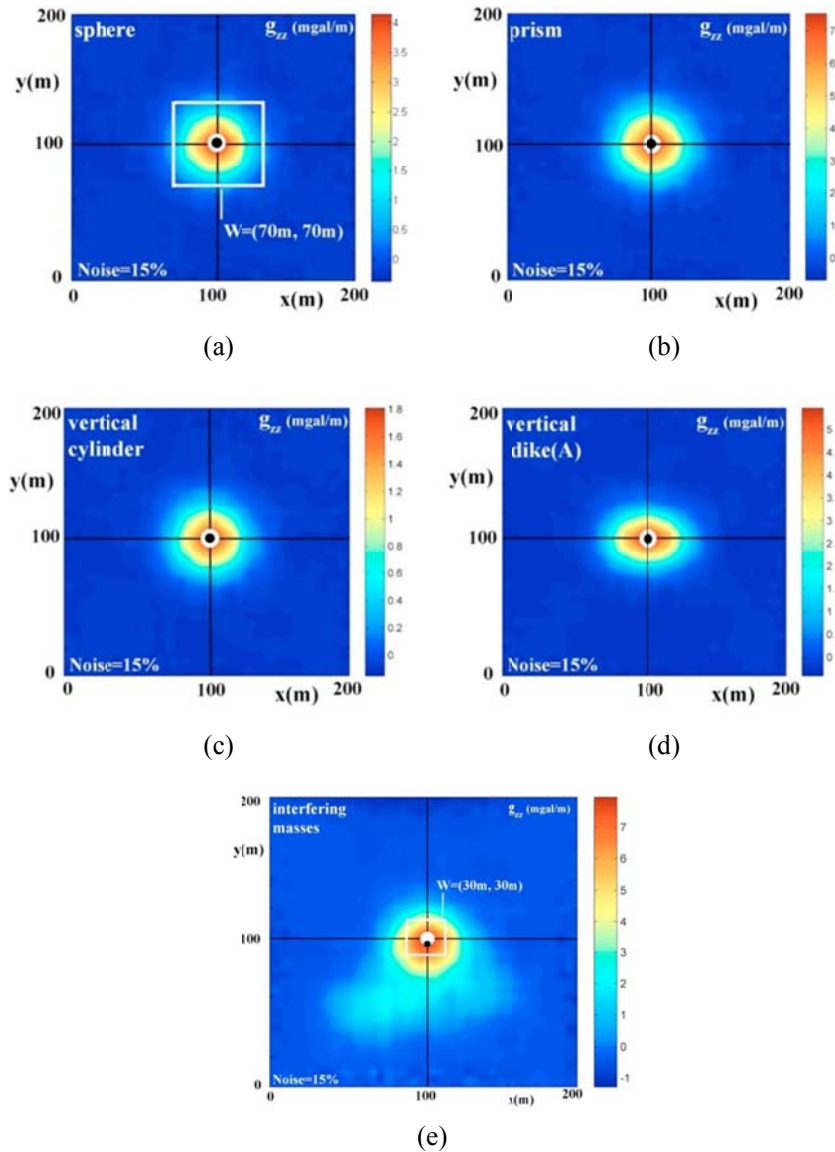


**Figure 2.** Smoothed  $g_{zz}$  component of the CGGT in the presence of 15% random Gaussian noise for: a) sphere; b) prism; c) vertical cylinder; d) vertical dike (A); e) a binary system. White circles show real COMs and black ones are the best estimated locations of COM. Deviation of black circle toward the adjacent model in (e) is obvious.

#### 4-2. Two dimensional bodies

In this section, a long horizontal cylinder and a vertical dike (B), as solitary models, are examined (see Table 1 and models (5) and (6) in Figure 1(a)). These models are representatives of 2D bodies. For extracting the solutions of the horizontal cylinder and influence of window shapes on them, three types of windows are considered: square window ( $W_{1,c}$ ), rectangular window ( $W_{2,c}$ ) with the length two times longer than its width, rectangular window ( $W_{3,c}$ ) with the length four times longer than its width. Since for a 2D body the maximum of  $g_{zz}$  is a line,

not a point, the center of the window could be positioned anywhere on this line except the edges. For a 2D mass, the rectangular window,  $W_{3,c}$ , gives the best solution with MSE, whereas square windows are suitable for 3D masses. The third eigenvector at the window center specifies the strike of the model. Figure 3(a) indicates  $g_{zz}$  contour map of the horizontal cylinder in a noisy condition (15%). For the vertical dike (B),  $I=0.12$  is indicative of a 2D body. The estimated strike direction approximates the real orientation of the dike very well. The results are shown in Table 1 and Figure 3(b).

At the last stage of analyzing synthetic models, the interfering effect of two transversely horizontal cylinders in different depths is studied (Figure 1(c)). The centers of horizontal cylinder (A) and (B) are in (100m, 100m, 20m) and (100m, 100m, 40m), respectively (Table 1). Since " $I=0.39$ " is less than the threshold value (0.5), the binary system is regarded as a quasi-2D model. In Figure 3(c), the  $g_{zz}$  map together with the window and the estimated strike direction are shown. The solution for the binary system indicates that the characteristics of the upper cylinder (its field) are stronger in the data than the lower one. The white circle is representative of real and black one indicates estimated COM of the system.

### 5. Case study

One of the most famous oil fields of the United States is Humble Oil Field.

Reservoir rocks of this area are andesitic and limestone rocks. For more information about geology refer to Nettleton (1962). Nettleton (1976) and Abdelrahman and El-Araby (1996) used the Bouguer gravity data in this area (Nettleton, 1962) and estimated the depth component of a salt dome as 4.97 km and 4.60 km, respectively. Constituting CGGT components from this Bouguer gravity data, the best extracted solution by our method was resulted from a window,  $W_f$ , with dimensions of 5.5 km $\times$ 5.5 km bearing 121 data points. The approximated  $I$  and MSE values were, in turn, 0.99 and 1.08%. Figure 4 indicates  $g_{zz}$  contour map of this geologic structure, the estimated COM of which was ( $X=17.47\pm 0.01$  km,  $Y=12.11\pm 0.01$  km,  $Z=4.61\pm 0.04$  km). The black circle and  $W_f$  in Figure 4 show this best estimated solution and window, in turn.

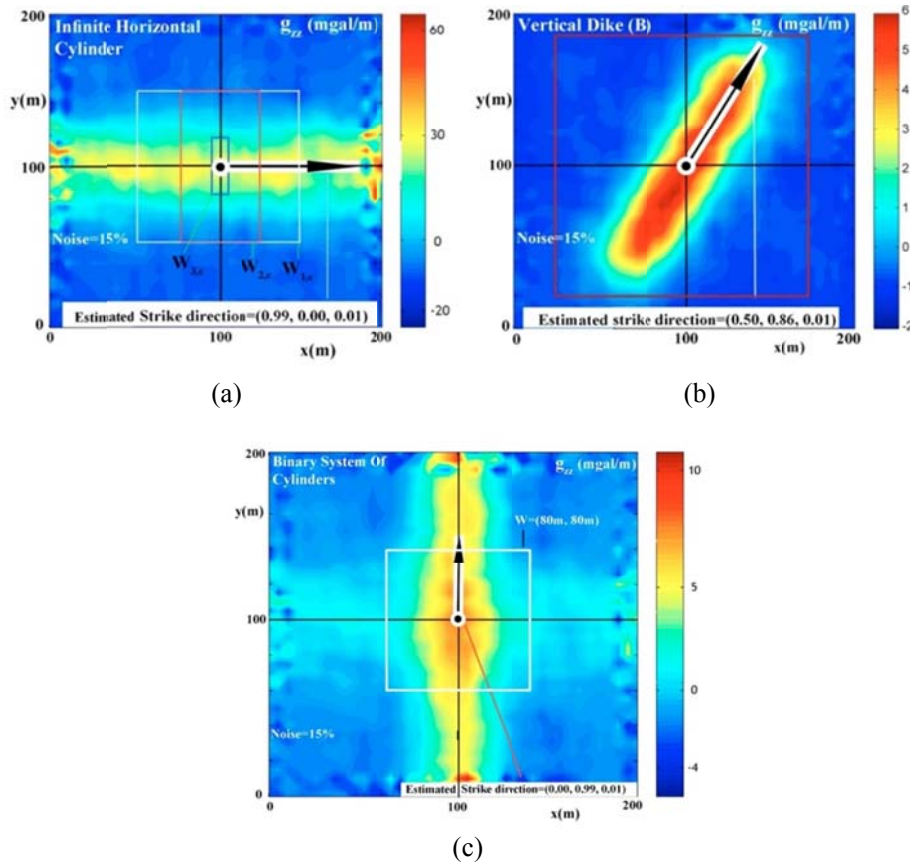


**Figure 3.** Smoothed  $g_{zz}$  component of the CGGT in presence of 15% noise for: a) infinite horizontal cylinder with strike direction of  $0^\circ$  (relative to x axis) along with its three types of windows; b) vertical dike (B) with strike direction of  $60^\circ$  (relative to x axis); c) a binary system of cylinders. White circles are real COMs, black ones are the best estimated locations and the vectors in the center of the windows at ( $x_{\max}=100\text{m}$ ,  $y_{\max}=100\text{m}$ ) indicate the estimated strike directions.

In the methods presented by Nettelton (1976) and Abdelrahman and El-Araby (1996), the horizontal location of COM was not discussed. However, the horizontal components of COM could be pinpointed quantitatively by our methodology. Additionally, even though Humble area appeared to be a noise free region, they did not discuss and regard the effect of noise in their offered techniques to extend them to other surveys in different regions. By contrast, noise effect constitutes considerable contents of our approach. Furthermore, the attained  $I=0.99$  in our methodology indicates that the mass is almost a pure 3-D mass. It is noteworthy that in the case of simulated data, Abdelrahman and El-Araby examined isolated, simple shaped and noiseless models, while our methodology serves to complex, noisy, solitary and interfering sources. The models are also analyzed in three dimensions, unlike those that published their work in two dimensions.

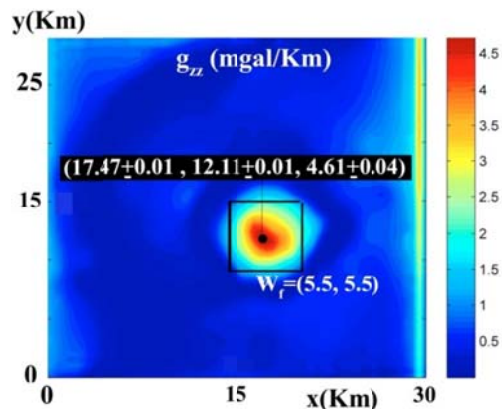


**Figure 4.**  $g_{zz}$  component of CGGT for a salt dome, near Humble city, USA. The dimensions of the most suitable window are 5.5 km×5.5 km including 121 data points. Black circle represents the estimated COM.

## 6. Conclusion

Integrating Hilbert Transform, gravity derivative calculations and least square procedure, this paper presents an independent approach to heighten the gravity interpretation process. Although the noise resistance of this methodology (after imposing Moving Twenty-five Point Averaging and Upward Continuation) might be slightly lower than the one presented by Beiki and Pedersen (2010), its obtained solutions for both solitary and binary models

are still fairly accurate. There are some privileges in employing this methodology. Definitely, it could save us time, energy and money. It also gives rise to more accurate and dependable results and enhances the quality of gravimetry interpretations. In fact, by measuring  $g_z$  (Bouguer gravity data) to any purpose, an additional strategy to analyze the data with higher resolution (because of using the gravity field derivatives) without extra expenses, time and field work is provided. Sometimes, the only available gravity data is just  $g_z$ , and employing this technique could give us much more valuable information, because, apart from COM, further knowledge about a causative body's dimensions and strike direction is yielded that may not be obtained precisely through routine Bouguer gravity data.

## References

- Abdelrahman, E. M. and El-Araby, T. M., 1996, Shape and depth solutions from moving average residual gravity anomalies. *Journal of Applied Geophysics*, 36, 89-95.
- Aster, R. C., Borchers, B. and Thurber, C., 2003, *Parameter Estimation and Inverse Problems*. Elsevier.
- Bell, R. E., Anderson, R. and Pratson, L., 1997, Gravity gradiometry resurfaces. *The Leading Edge*, 16, 55-59.
- Bell, R. E. and Hansen, R. O., 1998, The rise and fall of early oil field technology: The torsion balance gradiometer. *The Leading Edge*, 17, 81-83.
- Beiki, M. and Pedersen, L. B., 2010, Eigenvector analysis of the gravity gradient tensor to locate geologic bodies. *Geophysics*, 75(6), I37-I49.
- Childers, V. A., Bell, R. E. and Brozena, J. M., 1999, Airborne gravimetry: An investigation of filtering. *Geophysics*, 64, 61-69.
- Dransfield, M. H., 2007, Airborne gravity gradiometry in the research for mineral deposits. *Proceedings of Exploration 07: Fifth Decennial International Conference on Mineral Exploration*, edited by Milkereit, B., 341-354.
- Droujinine, A., Vasilevsky, A. and Evans, R., 2007, Feasibility of using full tensor gradient FTG data for detection of local lateral density contrasts during reservoir

- monitoring. *Geophysical Journal International*, 169, 795–820.
- Edwards, A. J., J. Maki, T. and Peterson, D. G., 1997, Gravity gradiometry as a tool for underground facility detection. *Journal of Environmental & Engineering Geophysics*, 2(2), 137–143.
- Fedi, M., Ferranti, L., Florio, G., Giori, I. and Italiano, F., 2005, Understanding the structural setting in the southern Apennines Italy: Insight from gravity gradient tensor. *Tectonophysics*, 397(1–2), 21–36.
- Fitz Gerald, D., Argast, D., Paterson, R. and Holstein, H., 2009, Full tensor magnetic gradiometry processing and interpretation developments. 11<sup>th</sup> South African Geophysical Association SAGA.
- Hatch, D., 2004, Evaluation of a full tensor gravity gradiometer for kimberlite exploration. The ASEG-PESA Airborne gravity workshop, Extended Abstracts, 73–80.
- Hinojosa, J. H. and Mickus, K. L., 2002, Hilbert transform of gravity gradient profiles: Special cases of the general gravity-gradient tensor in the Fourier transform domain. *Geophysics*, 67(3), 766–769.
- Mikhailov, V., Pajot, G., Diament, M. and Price, A., 2007, Tensor deconvolution: A method to locate equivalent sources from full tensor gravity data. *Geophysics*, 72(5), 161–169.
- Murphy, C. A. and Brewster, J., 2007, Target delineation using full tensor gravity gradiometry data. Extended Abstract, ASEG-PESA 19th International Geophysical Conference and Exhibition, Perth, Australia.
- Nabighian, M. N., 1984, Toward a three-dimensional automatic interpretation of potential field data via generalized Hilbert transforms: Fundamental relations. *Geophysics*, 49(6), 780–786.
- Nettleton, L. L., 1962, Gravity and magnetic for geologists and seismologists. *AAPG Bulletin*, 46, 1815–1838.
- Nettleton, L. L., 1976, Gravity and Magnetism in oil prospecting. McGraw-Hill, New York.
- Oruc, B., 2010, Depth Estimation of Simple Causative Sources from Gravity Gradient Tensor Invariants and Vertical Component. *Pure. Appl. Geophys.* 167, 1259–1272.
- Pajot, G., de Viron, O., Diament, M., Lequentrec-Lalancette, M. F. and Mikhailov, V., 2008, Noise reduction through joint processing of gravity and gravity gradient data. *Geophysics*, 73(3), 123–134.
- Pedersen, L. B. and Rasmussen, T. M., 1990, The gradient tensor of potential field anomalies: Some implications on data collection and data processing of maps. *Geophysics*, 55, 1558–1566.
- Pawlowski, B., 1998, Gravity gradiometry in resource exploration. *The Leading Edge*, 17, 51–52.
- Routh, P., Jorgensen, G. J. and Kisabeth, J. L., 2001, Base of the salt mapping using gravity and tensor gravity data. 70th Annual International Meeting, SEG, Expanded Abstracts, 1482–1484.
- Vasco, O. W. and Taylor, C., 1991, Inversion of airborne gravity gradient data, southwestern Oklahoma. *Geophysics*, 56, 90–91.
- While, J., Biegert, E. and Jackson, A., 2009, Generalized sampling interpolation of noise gravity/gravity gradient data. *Geophysical Journal International*, 178, 638–650.
- While, J., Jackson, A., Smit, D. and Biegert, E., 2006, Spectral analysis of gravity gradiometry profiles. *Geophysics*, 71(1), J11–J22.
- Zhdanov, M. S., Ellis, R. and Mukherjee, S., 2004, Three-dimensional regularized focusing inversion of gravity gradient tensor component data. *Geophysics*, 69, 925–937.
- Zhang, C., Mushayandebvu, M. F., Reid, A. B., Fairhead, J. D. and Odegard, M., 2000, Euler deconvolution of gravity tensor gradient data. *Geophysics*, 65, 512–520.
- Zhou, W., 2016, Depth Estimation Method Based on the Ratio of Gravity and Full Tensor Gradient Invariant. *Pure. Appl. Geophys.* 173(2), 499–508.